The Astrophysical Journal Letters, 988:L68 (11pp), 2025 August 1 https://doi.org/10.3847/2041-8213/aded07

Cooling Regimes of Nonthermal Electrons: The Slow, the Fast, and the Very Fast

Sk. Minhajur Rahaman[1], Jonathan Granot[1,2,3], and Paz Beniamini[1,2,3]
[1] Astrophysics Research Center of the Open University (ARCO), The Open University of Israel, P.O Box 808, Ra'anana 4353701, Israel
[2] Department of Natural Sciences, The Open University of Israel, P.O Box 808, Ra'anana 4353701, Israel
[3] Department of Physics, The George Washington University, 725 21st Street NW, Washington, DC 20052, USA
Received 2025 June 8; revised 2025 July 3; accepted 2025 July 7; published 2025 July 30

Abstract

In many astrophysical systems, nonthermal radiation is emitted by accelerated charged particles, whose cooling rates play a crucial role in determining their luminosity and spectral properties. We consider synchrotron radiation from a power-law energy distribution of relativistic electrons and provide a comprehensive framework for understanding particle cooling regimes, focusing on the fast cooling (FC) and very fast cooling (VFC) regimes. In FC, all electrons cool significantly on the dynamical time but remain relativistic. In VFC, all electrons cool to nonrelativistic speeds much faster than the dynamical time. The VFC regime is realized only in highly relativistic sources, with no Newtonian counterpart. It is highly relevant for the prompt phase of gamma-ray bursts (GRBs), where it can naturally occur regardless of the dissipation mechanism and with weak dependence on the degree of magnetization. We find that the FC and VFC regimes are satisfied in a broad range of parameters, under which bright optical emission can be observed during the prompt GRB phase. The brightest optical emission corresponds to an unbroken power-law spectrum extending from the sub-MeV peak of the bolometric luminosity to optical/UV frequencies. Additionally, we propose that VFC in the Thomson-thick regime is necessary for producing a bright and narrow electron–positron annihilation line, as was observed in the B.O.A.T. event, GRB 221009A.

Unified Astronomy Thesaurus concepts: Relativistic jets (1390); Non-thermal radiation sources (1119); Gamma-ray bursts (629); Optical observation (1169)

1. Introduction

Nonthermal emission is prevalent across various astrophysical sources, ranging from Newtonian systems like supernovae, to subrelativistic sources such as pulsar wind nebulae, to mildly relativistic phenomena like magnetar giant flares, to ultrarelativistic sources, including blazars and gamma-ray bursts (GRBs). Such emission arises from nonthermal particles accelerated through reconnection events or shock heating. The power and spectral characteristics of their emission are governed by the energy-loss mechanisms of the particles. In this work, we focus on synchrotron radiation from relativistic electrons that are accelerated into a power-law energy distribution. While most studies (R. Sari et al. 1998; J. Granot et al. 2000) focus on fast cooling (FC) or slow cooling (SC) regimes, this work emphasizes the importance of the very fast cooling (VFC) regime, first introduced by D. Guetta & J. Granot (2003).

The Letter is organized as follows. Section 2 expands on cooling regimes with a special emphasis on VFC. Section 3 focuses on the application of the synchrotron self-absorption effects in GRB prompt emission. Section 4 focuses on the role of a VFC regime in the origin of the multi-MeV line in GRB 221009A. Section 5 qualitatively explores the impact of particle cooling on reconnection events. Finally, Section 6 summarizes the main conclusions of this work.

2. Cooling Regimes

We present an overview of the cooling regimes of nonthermal particles, characterized by a power-law distribution with index p and bounded by the minimal and maximal Lorentz factors (LFs; $\gamma_{\rm m}$, $\gamma_{\rm M}$). For ultrarelativistic sources, this distribution is described in the comoving frame, with physical quantities denoted as primed. We begin by describing a generic continual injection process that gives rise to this nonthermal distribution, followed by a description of the particle distribution and the corresponding photon spectrum, while excluding self-absorption effects. Our primary focus is on the VFC regime, placing it within the broader context of other cooling regimes. Although self-absorption is not discussed in this section, we will study its affects in Section 3, focusing on the implications for the VFC regime. For the rest of our analysis, $N_{\rm e}$ is the total number of electrons accelerated within one dynamical timescale, $t'_{\rm dyn}$. The radiative efficiency $\epsilon_{\rm rad}$ represents the fraction of energy lost to radiation by nonthermal electrons within $t'_{\rm dyn}$.

The setup of our system is as follows. An acceleration process injects *fresh* nonthermal relativistic electrons with a power-law energy distribution described by

$$\frac{dN}{d\gamma_{\rm e}} = K\gamma_{\rm e}^{-p} \text{ for } \gamma_{\rm m} \leqslant \gamma_{\rm e} \leqslant \gamma_{\rm M}\,, \tag{1}$$

where K ($=N_{\rm e}/(p-1)$ for $p > 2$ and $\gamma_{\rm M} \to \infty$) is a normalization constant and p is the power-law index. The LFs of the nonthermal particles $\gamma_{\rm e}$ are defined in the comoving frame. In our setup, we assume that the fresh electrons are instantaneously accelerated to the power-law distribution. The (comoving) cooling time $t'_{\rm c}$ of an electron with LF $\gamma_{\rm e}$ is defined

Table 1
Particle and Photon Spectrum in Different Cooling Regimes

Regime	Particle Distribution $\frac{dN}{d\gamma_e}$	Photon Spectrum $L_\nu/L_{\nu_{\max}}$	$\epsilon_{\rm rad}$	Dynamics
VSC	γ_e^{-p} for $\gamma_m < \gamma_e < \gamma_M$	$\begin{cases} \left(\frac{\nu}{\nu_m}\right)^{\frac{1}{3}} & \text{for } \nu_B < \nu < \nu_m \\ \left(\frac{\nu}{\nu_m}\right)^{-\frac{p-1}{2}} & \text{for } \nu_m < \nu < \nu_M \end{cases}$	$\begin{cases} \frac{\gamma_m}{\gamma_c} & \text{for } 3 < p \\ \frac{\gamma_M}{\gamma_c}\left(\frac{\gamma_M}{\gamma_m}\right)^{2-p} & \text{for } 2 < p < 3 \\ \frac{\gamma_M}{\gamma_c} & \text{for } p < 2 \end{cases}$	No
SC	$\begin{cases} \gamma_e^{-1-p} & \text{for } \gamma_c < \gamma_e < \gamma_M \\ \gamma_e^{-p} & \text{for } \gamma_m < \gamma_e < \gamma_c \end{cases}$	$\begin{cases} \left(\frac{\nu}{\nu_m}\right)^{\frac{1}{3}} & \text{for } \nu_B < \nu < \nu_m \\ \left(\frac{\nu}{\nu_m}\right)^{-\frac{p-1}{2}} & \text{for } \nu_m < \nu < \nu_c \\ \left(\frac{\nu_c}{\nu_m}\right)^{-\frac{p-1}{2}}\left(\frac{\nu}{\nu_c}\right)^{-\frac{p}{2}} & \text{for } \nu_c < \nu < \nu_M \end{cases}$	$\begin{cases} \frac{\gamma_m}{\gamma_c} & \text{for } 3 < p \\ \left(\frac{\gamma_c}{\gamma_m}\right)^{2-p} & \text{for } 2 < p < 3 \\ 1 & \text{for } p < 2 \end{cases}$	Yes ($p < 2$)
FC	$\begin{cases} \gamma_e^{-1-p} & \text{for } \gamma_m < \gamma_e < \gamma_M \\ \gamma_e^{-2} & \text{for } \gamma_c < \gamma_e < \gamma_m \end{cases}$	$\begin{cases} \left(\frac{\nu}{\nu_c}\right)^{\frac{1}{3}} & \text{for } \nu_B < \nu < \nu_c \\ \left(\frac{\nu}{\nu_c}\right)^{-\frac{1}{2}} & \text{for } \nu_c < \nu < \nu_m \\ \left(\frac{\nu_m}{\nu_c}\right)^{-\frac{1}{2}}\left(\frac{\nu}{\nu_m}\right)^{-\frac{p}{2}} & \text{for } \nu_m < \nu < \nu_M \end{cases}$	1	Yes
VFC	$\begin{cases} \gamma_e^{-1-p} & \text{for } \gamma_m < \gamma_e < \gamma_M \\ \gamma_e^{-2} & \text{for } 1 < \gamma_e < \gamma_m \end{cases}$	$\begin{cases} \bar{\gamma}_c\left(\frac{\nu}{\nu_B}\right)^{-\frac{1}{2}} & \text{for } \nu_B < \nu < \nu_m \\ \bar{\gamma}_c\left(\frac{\nu_m}{\nu_B}\right)^{-\frac{1}{2}}\left(\frac{\nu}{\nu_m}\right)^{-\frac{p}{2}} & \text{for } \nu_m < \nu < \nu_M \end{cases}$	1	Yes

Note. Summary of the different cooling regimes, particle distribution, emitted photon spectrum (without self-absorption effects), radiative efficiency $\epsilon_{\rm rad}$, and the effect of radiative cooling on the global dynamics. This table accompanies Figure 1.

as the ratio of its kinetic energy and radiated power,

$$t'_c(\gamma_e) = \frac{E}{\left(\frac{dE}{dt'}\right)} = \frac{(\gamma_e - 1)m_e c^2}{\frac{\sigma_T c B'^2}{6\pi}(\gamma_e^2 - 1)} = \frac{t'_{c1}}{\gamma_e + 1} \approx \frac{t'_{c1}}{\gamma_e}\,, \tag{2}$$

where $t'_{c1} = \frac{6\pi m_e c}{\sigma_T B'^2}$ is the synchrotron cooling timescale associated with a mildly relativistic electron with $\gamma_e \sim 1$ (see Appendix A). Here $-e$ and m_e are the charge and mass of the electron, B' is the comoving magnetic field strength, and c is the speed of light. In the power-law distribution, for $p > 2$, the low-energy electrons dominate both the total energy and the total number of electrons. However, for $1 < p < 2$, while the total number is still dominated by the low-energy electrons, the total energy is dominated by the high-energy and faster-cooling electrons. In this case, if the nonthermal electrons carry a significant fraction of the total energy in the outflowing material, radiative cooling of the particles may affect the overall dynamics of the outflow.

We further introduce the cooling times of electrons with the minimal and maximal LF in the accelerated power-law energy distribution, $t'_{cm} \equiv t'_c(\gamma_m) \approx t'_{c1}/\gamma_m$ and $t'_{cM} \equiv t'_c(\gamma_M) \approx t'_{c1}/\gamma_M$, respectively (note that $t'_{cM} < t'_{cm}$ since $\gamma_M > \gamma_m$.). If all electrons can cool within one dynamical timescale ($t'_{cm} < t'_{dyn}$; FC or VFC), then $\epsilon_{\rm rad} \approx 1$. However, $\epsilon_{\rm rad} \ll 1$ if $t'_{cM} > t'_{dyn}$ (very slow cooling, VSC) and $p < 2$ or if $t'_{cm} > t'_{dyn}$ (VSC or SC, where $t'_{cM} < t'_{dyn} < t'_{cm}$) and $p > 2$, since in both cases the electrons carrying most of the energy lose only a small fraction of their energy during one dynamical time (see Table 1 for expressions for $\epsilon_{\rm rad}$ in the relevant regime).

The electron cooling LF γ_c is defined as the LF to which an electron with $\gamma_M \to \infty$ cools to over one dynamical time. Note that this refers to electrons that contribute significantly to the observed emission, thus requiring $u_e = \gamma_e\beta_e \gtrsim 1$ and $u_c = (\gamma_c^2 - 1)^{1/2} \gtrsim 1$. It is convenient to introduce the parameter $\bar{\gamma}_c$ such that

$$\bar{\gamma}_c = \frac{t'_{c1}}{t'_{\rm dyn}}\,, \qquad \gamma_c \approx \max(1, \bar{\gamma}_c)\,. \tag{3}$$

While $\bar{\gamma}_c$ aligns with the cooling LF γ_c across most regimes, in the VFC regime, $\bar{\gamma}_c < 1$, and it does not represent a physical LF (owing to the nature of approximations made above only applicable for $\gamma \gg 1$) and $\gamma_c \approx 1$.

The source's maximum spectral luminosity (which is not the same as the peak of the bolometric luminosity νL_ν) is determined by the product of the instantaneous number $N_{\rm inst}$ of relativistic electrons and the maximum spectral power $P_{\nu,\max} \approx m_e c^2 \sigma_T B/3e$ due to each electron.[4] It is given as

$$\begin{aligned} L_{\nu,\max} &= N_{\rm inst} P_{\nu,\max} \\ &= \begin{cases} N_e P_{\nu,\max} & \text{at } \nu_m \text{ for } \bar{\gamma}_c > \gamma_m \text{ (SC)} \\ N_e P_{\nu,\max} & \text{at } \nu_c \text{ for } 1 < \bar{\gamma}_c < \gamma_m \text{ (FC)}, \\ \bar{\gamma}_c N_e P_{\nu,\max} & \text{at } \nu_B \text{ for } \bar{\gamma}_c < 1 \text{ (VFC)} \end{cases} \end{aligned} \tag{4}$$

which shows that for VFC, $\bar{\gamma}_c$ is still meaningful, as it indicates that only a small fraction $N_{\rm inst} = \bar{\gamma}_c N_e$ of the total nonthermal electrons N_e accelerated over one dynamical timescale contribute to the instantaneous emission.

[4] A similar approach can also be extended to emission above the synchrotron peak (see the discussion in P. Beniamini & T. Piran 2013, particularly around Equation (11) and Figure 1).

The characteristic synchrotron frequencies in the observer frame—namely, the minimal ($\nu_{\rm m}$), cooling ($\nu_{\rm c}$), modified cooling ($\bar{\nu}_{\rm c}$; unphysical in the VFC regime), and maximal ($\nu_{\rm M}$) frequencies—can all be expressed in the unified form

$$\nu_X = \nu_{\rm B}\gamma_X^2 \,, \tag{5}$$

where γ_X stands for any of the corresponding electron LFs: $\gamma_{\rm m}$, $\gamma_{\rm c}$, $\bar{\gamma}_{\rm c}$, or $\gamma_{\rm M}$. The characteristic synchrotron frequency scale is given by

$$\nu_{\rm B} = \frac{\mathcal{D}\nu'_{\rm B}}{1+z} \,, \quad \text{with} \quad \nu'_{\rm B} = \frac{eB'}{2\pi m_{\rm e}c} \,, \tag{6}$$

where B' is the comoving magnetic field, $\nu_{\rm B}$ is the cyclotron frequency ($\nu'_{\rm B}$ in the comoving frame), z is the source's cosmological redshift, $\mathcal{D} = 1/\Gamma(1-\beta\mu)$ is the Doppler factor, and $\mu \equiv \cos\theta$, where θ is the angle between the bulk velocity vector (βc) of the emitting plasma and our line of sight. For the rest of the analysis, for relativistic sources, we assume that, due to relativistic beaming, only radiation within a $1/\Gamma$ cone around the line of sight contributes significantly to the observed emission. This translates to the approximation $\mathcal{D} \approx \Gamma$.

The ordering of $\gamma_{\rm m}$, $\bar{\gamma}_{\rm c}$, and 1 dictates the specific cooling regime. Figure 1 and the accompanying Table 1 in Appendix B summarize the particle distribution and corresponding photon spectrum, excluding self-absorption effects. Below, we provide a brief description of these regimes.

VSC ($1 < \gamma_{\rm m} < \gamma_{\rm M} < \bar{\gamma}_{\rm c} = \gamma_{\rm c}$). In this regime, the cooling LF, $\gamma_{\rm c} = \bar{\gamma}_{\rm c}$, is larger than both $\gamma_{\rm m}$ and $\gamma_{\rm M}$, meaning that none of the electrons in the nonthermal distribution have enough time to cool within the dynamical timescale. As a result, the radiative efficiency is very low, $\epsilon_{\rm rad} \ll 1$, and radiative losses do not significantly affect the global dynamics.

SC ($1 < \gamma_{\rm m} < \bar{\gamma}_{\rm c} = \gamma_{\rm c} < \gamma_{\rm M}$). In the SC regime, the cooling LF, $\gamma_{\rm c} = \bar{\gamma}_{\rm c}$, lies between $\gamma_{\rm m}$ and $\gamma_{\rm M}$. Only electrons with LFs between $\bar{\gamma}_{\rm c}$ and $\gamma_{\rm M}$ significantly cool within one dynamical time, while lower-energy electrons remain uncooled. The radiative efficiency is low ($\epsilon_{\rm rad} \ll 1$) for $p > 2$, but for $p < 2$, it becomes high ($\epsilon_{\rm rad} \approx 1$) and can significantly affect the global dynamics of the outflow (or system).

Marginally FC ($1 < \bar{\gamma}_{\rm c} = \gamma_{\rm c} = \gamma_{\rm m} < \gamma_{\rm M}$; *not shown in Figure 1 and Table 1*). This regime marks the boundary between FC and SC (G. Ghisellini & A. Celotti 1999; P. Kumar & E. McMahon 2008; F. Daigne et al. 2011; P. Beniamini et al. 2018). Here, the cooling LF, $\gamma_{\rm c} = \bar{\gamma}_{\rm c}$, equals $\gamma_{\rm m}$, meaning that most electrons (for $p > 1$) cool just on the dynamical timescale. This regime is particularly attractive for modeling the prompt emission of GRBs, as it permits the maintenance of high radiative efficiency while simultaneously yielding a relatively hard low-energy spectral slope with a particle distribution index $p > 2$.

FC ($1 < \bar{\gamma}_{\rm c} = \gamma_{\rm c} < \gamma_{\rm m} < \gamma_{\rm M}$). In the FC regime, $\gamma_{\rm c} = \bar{\gamma}_{\rm c}$ is lower than $\gamma_{\rm m}$. All electrons cool down to $\bar{\gamma}_{\rm c}$ within the dynamical timescale, resulting in a radiative efficiency of approximately unity, $\epsilon_{\rm rad} \approx 1$, and the overall dynamics may be affected.

VFC ($\bar{\gamma}_{\rm c} \ll \gamma_{\rm c} \sim \sqrt{2} < \gamma_{\rm m} < \gamma_{\rm M}$). In this regime, $\bar{\gamma}_{\rm c}$ is much smaller than 1, meaning that electrons cool to nonrelativistic speeds on timescales much shorter than the dynamical timescale (D. Guetta & J. Granot 2003). Although

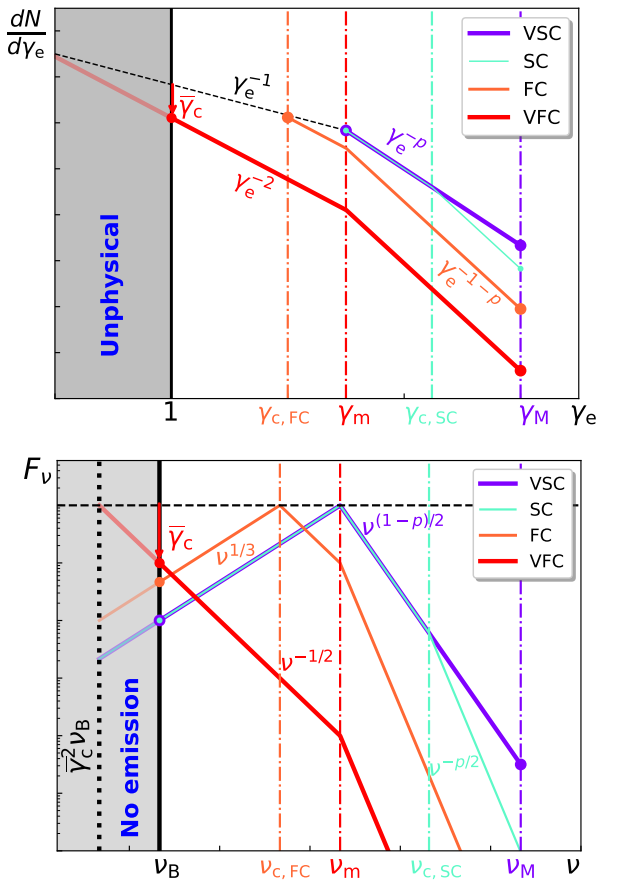

Figure 1. Schematic log–log plots of the particle energy distribution (top panel) and the emitted spectrum (bottom panel) after one dynamical timescale. Injected electrons follow a power-law distribution with index p, bounded by minimum and maximum LFs, $\gamma_{\rm m}$ and $\gamma_{\rm M}$, respectively. The photon spectrum excludes self-absorption, and Table 1 in Appendix B summarizes the scaling relations. Red, orange, cyan, and purple lines represent the VFC, FC, SC, and VSC regimes, respectively. Top panel: the number density of nonthermal electrons as a function of LF (log–log scale). The vertical black line marks $\gamma_{\rm e} = 1$. The red and purple dotted–dashed lines indicate $\gamma_{\rm m}$ and $\gamma_{\rm M}$, while the red arrow shows the fraction of electrons contributing to emission in the VFC regime. The orange and cyan dotted–dashed lines mark the cooling LF $\gamma_{\rm c}$ for the FC and SC regimes, and the black dotted line traces the cooling LF in the FC regime. Bottom panel: the flux density as a function of frequency. The vertical black line marks the cyclotron frequency, $\nu_{\rm B}$, and the shaded region represents an emission-free zone. The dotted black line indicates the (unphysical) VFC cooling frequency. The orange, red, cyan, and purple lines marking the FC cooling frequency, minimal frequency, SC cooling frequency, and maximum synchrotron frequency, respectively.

$\bar{\gamma}_{\rm c} \ll 1$ does not correspond to a physical LF, it represents the fraction of nonthermal electrons contributing to the instantaneous emission, such that only a small fraction of electrons (the instantaneously relativistic ones) are responsible for the observed emission at any given time. In this regime, the radiative efficiency is effectively unity ($\epsilon_{\rm rad} = 1$), as all electrons lose their energy almost instantaneously. As for FC, the overall dynamics may be affected (see Section 5).

To summarize, one of the highlights of this work is the introduction of the generalized cooling LF $\bar{\gamma}_{\rm c}$, representing the typical cooling LF $\gamma_{\rm c}$ across most regimes, except for the VFC regime, where $\bar{\gamma}_{\rm c}$ does not correspond to a physical LF but indicates a small fraction of the total nonthermal electrons that contribute to the instantaneous emission. In the next section, we will explore the conditions for VFC to be realized in highly relativistic astrophysical outflows.

3. Self-absorption Effects in Relativistic Outflows

In this section, we focus on self-absorption effects in ultrarelativistic outflows relevant to the prompt phase of GRBs. In particular, we investigate which particle cooling regime—FC or SC—is more conducive to the detection of prompt optical continuum emission that is temporally coincident with the prompt gamma-ray emission.

Consider a relativistic outflow with LF Γ, equivalent isotropic power $L_{\rm j,iso}$, and magnetization $\sigma \equiv \frac{B'^2}{4\pi h\rho' c^2}$ (where h is the dimensionless specific enthalpy). The electromagnetic power flowing across a spherical surface of radius R can be expressed as $L_{\rm EM} = \frac{\sigma}{1+\sigma} L_{\rm j,iso} = 4\pi R^2 S = R^2 B'^2 \Gamma^2 \beta c$, where $S = |\boldsymbol{S}|$, $\boldsymbol{S} = \frac{c}{4\pi}\boldsymbol{E} \times \boldsymbol{B}$ being the Poynting flux (where $\boldsymbol{E}$ and $\boldsymbol{B}$ are the electric and magnetic fields associated with the flow). We parameterize the magnetization $\sigma(R)$ in the jet as a function of the distance R from the central engine. Two dissipation sites are associated with relativistic jets: an external dissipation site $R_{\rm ext}$ far from the central source and an internal dissipation site $R_{\rm o}$ closer to the source. Let a generic internal dissipation process within an ultrarelativistic outflow convert an effective fraction ϵ of the isotropic equivalent jet power $L_{\rm j,iso}$ into isotropic equivalent radiation $L_{\rm iso}$ at a distance $R_{\rm o}$. We denote the magnetization after dissipation at radius $R_{\rm o}$ as $\sigma = \sigma(R_{\rm o})$. The efficiency factor $\epsilon \equiv L_{\rm iso}/L_{\rm j,iso}$ is the product of three efficiencies: $\epsilon = \epsilon_{\rm th}\epsilon_{\rm e}\epsilon_{\rm rad}$, where $\epsilon_{\rm th}$ is the fraction of total power converted into internal energy, $\epsilon_{\rm e}$ is the fraction of internal energy imparted to the nonthermal electrons, and $\epsilon_{\rm rad}$ is the fraction of their energy that these electrons radiate. For convenience, we also define $\bar{\epsilon} \equiv \epsilon_{\rm th}\,\epsilon_{\rm e} = \epsilon/\epsilon_{\rm rad}$. The dissipation radius is related to the observed cosmological rest-frame variability time $t_{\rm vz}$ through $R_{\rm o} \approx f\Gamma^2 c t_{\rm vz}$, where the radius scaling factor f depends on the specifics of the dissipation process. For internal shocks, this factor can be approximated as $f \approx 2$ for collision of fast and slow material with very high proper-speed contrast (S. M. Rahaman et al. 2024). As another example, in reconnection models that produce relativistic plasmoid motion in the bulk frame, one typically finds $f \sim 2\Gamma'$, with $\Gamma' \lesssim 10$ (P. Beniamini & J. Granot 2016). The dynamical time is defined as the comoving radius doubling time, given by $t'_{\rm dyn} = \frac{R}{\Gamma c} = f\Gamma t_{\rm vz}$. The critical $\bar{\gamma}_{\rm c}$ can be expressed in terms of the observables $L_{\rm iso}$ and $t_{\rm vz}$ for $\epsilon_{\rm rad} \approx 1$ (VFC, FC, or SC with $p < 2$) as follows:

$$\bar{\gamma}_{\rm c}(\epsilon_{\rm rad} = 1) \equiv \bar{\gamma}_{\rm c,0} = \left(\frac{6\pi m_{\rm e} c^4}{\sigma_{\rm T}}\right)\frac{(1+\sigma)\bar{\epsilon}}{\sigma L_{\rm iso}}\Gamma^5 f t_{\rm vz}\,. \quad (7)$$

More generally, one needs to solve the equation $\bar{\gamma}_{\rm c} = \bar{\gamma}_{\rm c,0}\epsilon_{\rm rad}(\bar{\gamma}_{\rm c})$ for $\bar{\gamma}_{\rm c}$, and we provide the results for the different cases in Table 2.

Moreover, a critical factor that decides whether the postdissipation radiation is generated in an optically thick or optically thin regime is the location of the photospheric radius $R_{\rm ph}$. Below $R_{\rm ph}$, the dissipation is subphotospheric (optically thick), and vice versa. Next, we estimate the contribution of baryonic electrons in the outflow to the optical depth. The comoving number density of the baryonic electrons is $n'_{\rm e} = \frac{L_{\rm j,iso}/(1+\sigma)}{4\pi R^2\Gamma^2\beta m_{\rm p} c^3}$. The causal size associated with a relativistic source is $\Delta R' = \frac{R}{c\Gamma}$. The Thomson optical depth due to these baryonic electrons $\tau_{\rm T} = n'_{\rm e}\sigma_{\rm T}\Delta R'$. The photospheric radius $R_{\rm ph}$ is defined as the radius for which the optical depth equals unity, $\tau_{\rm T} = 1$. For the given jet parameters (σ, ϵ, $\gamma_{\rm m}$), we can define a number of critical LFs as

$$\begin{aligned}\Gamma_\tau &\equiv \Gamma(\tau_{\rm T} = 1)\\ &\approx 90\left(\frac{L_{52}}{((1+\sigma_{-1})/1.1)\,\bar{\epsilon}_{-0.3} f_{0.3}\, t_{-1}}\right)^{1/5}\\ &\approx 0.38\;\Gamma_{\rm c1}\;\bar{\epsilon}_{-0.3}^{\,1/5}\;\sigma_{-1}^{-1/5}\,, \end{aligned} \quad (8)$$

$$\begin{aligned}\Gamma_{\rm c1} &\equiv \Gamma(\bar{\gamma}_{\rm c} = 1)\\ &\approx 235\left(\frac{\sigma_{-1} L_{52}}{((1+\sigma_{-1})/1.1)\,\bar{\epsilon}_{-0.3} f_{0.3}\, t_{-1}}\right)^{1/5}, \end{aligned} \quad (9)$$

$$\begin{aligned}\Gamma_{\rm cm} &\equiv \Gamma(\bar{\gamma}_{\rm c} = \gamma_{\rm m})\\ &\approx 1700\left(\frac{\sigma_{-1}\gamma_{\rm m,4.3} L_{52}}{((1+\sigma_{-1})/1.1)\,\bar{\epsilon}_{-0.5} f_{0.3}\, t_{-1}}\right)^{1/5}. \end{aligned} \quad (10)$$

Here $\sigma_{-1} = \sigma/0.1$, $\bar{\epsilon}_{-0.5} = \bar{\epsilon}/0.2$, $f_{0.3} = f/2$, $L_{52} = L_{\rm iso}/10^{52}$ erg s^{-1}, and $t_{-1} = t_{\rm vz}/0.1$ s. Equation (9) shows that VFC is guaranteed for $\Gamma < \Gamma_{\rm c1}$ with a very weak dependence on ($L_{\rm iso}$, $t_{\rm vz}$, f, ϵ).

Equation (8) demonstrates that Γ_τ is always smaller than $\Gamma_{\rm c1}$, implying the existence of a parameter space where VFC can occur in relativistic outflows within the optically thin regime. For a fixed variability timescale, isotropic luminosity, jet magnetization, and efficiency of the conversion of jet power into radiation, the relative order of Γ, $\Gamma_{\rm c1}$, and Γ_τ determines the operating regime of the VFC. When $\Gamma < \Gamma_\tau$, VFC occurs in the optically thick (subphotospheric) regime, where radiation is affected by propagation effects; although this regime is not the focus of the current work, it is addressed in a companion study on the origin of the electron–positron annihilation line in GRB 221009A and briefly mentioned in Section 4. Conversely, when $\Gamma_\tau < \Gamma < \Gamma_{c1}$, VFC operates in the optically thin regime, which lacks a Newtonian counterpart, as discussed in Appendix C.

Next, we explore the observational implications of different electron cooling regimes for the optical emission accompanying the prompt phase of GRBs. We adopt the shock acceleration and cooling framework developed by J. Granot et al. (2000) and J. Granot & R. Sari (2002), which models the nonthermal electron population following the dissipation event that produces the prompt emission (see Appendix D for discussion of alternative one-zone models).

Table 2
Generalized Cooling LF $\bar{\gamma}_{\rm c}$ in the SC and VSC Regimes

Cooling Regime	Expression for $\bar{\gamma}_{\rm c}$	
SC	$\begin{cases}\sqrt{\bar{\gamma}_{\rm c,0}\gamma_{\rm m}} & \text{for } 3 < p\\ \gamma_{\rm m}^{\frac{p-2}{p-1}}\,\bar{\gamma}_{\rm c,0}^{\frac{1}{p-1}} & \text{for } 2 < p < 3\\ \bar{\gamma}_{\rm c,0} & \text{for } p < 2\end{cases}$	
VSC	$\begin{cases}\sqrt{\bar{\gamma}_{\rm c,0}\gamma_{\rm m}} & \text{for } 3 < p\\ \sqrt{\bar{\gamma}_{\rm c,0}\gamma_{\rm M}}\left(\frac{\gamma_{\rm M}}{\gamma_{\rm m}}\right)^{\frac{2-p}{2}} & \text{for } 2 < p < 3\\ \sqrt{\bar{\gamma}_{\rm c,0}\gamma_{\rm M}} & \text{for } p < 2\end{cases}$	

Note. The expression for $\bar{\gamma}_{\rm c,0}$ is given in Equation (7).

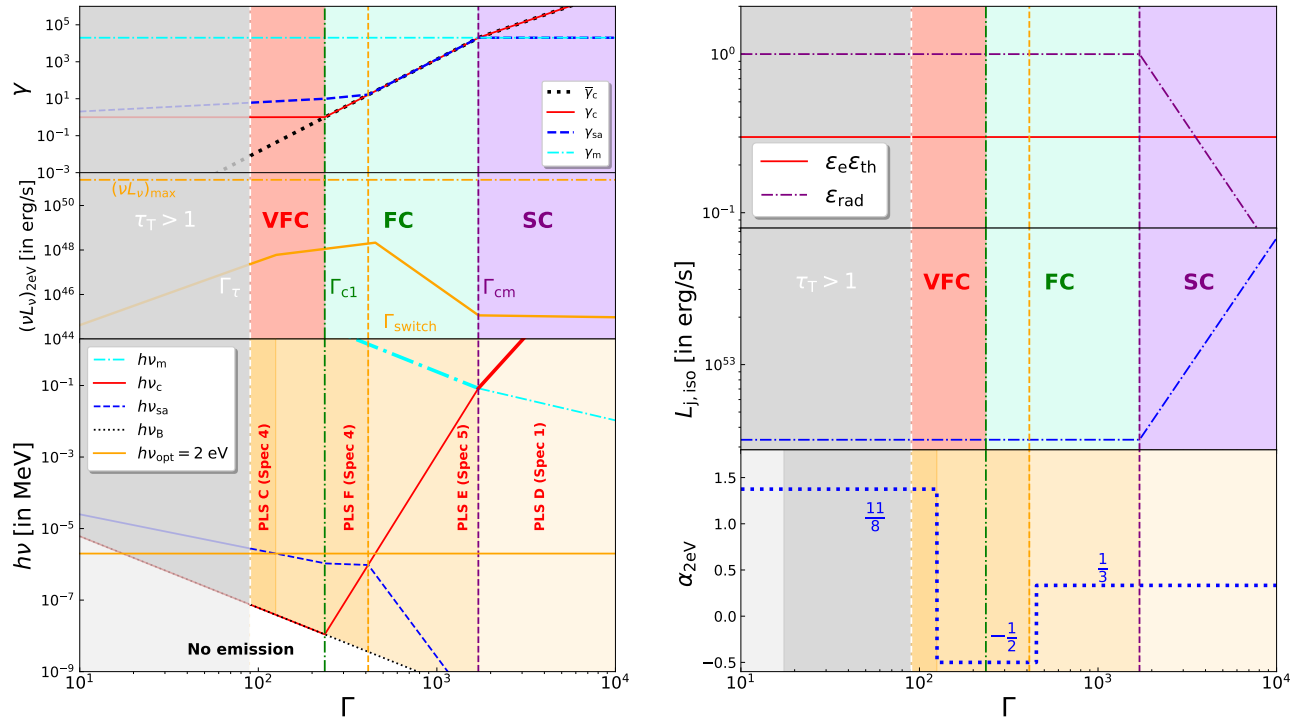

Figure 2. Effect of synchrotron self-absorption on prompt-phase optical emission in GRBs. The following parameters are fixed: isotropic observed luminosity $L_{\rm iso} = 10^{52}$ erg s^{-1}, radius scaling factor $f = 2$, variability timescale $t_{\rm vz} = 0.1$ s, jet magnetization $\sigma = 0.1$, electron power-law index $p = 2.5$, and minimal comoving LF $\gamma_{\rm m} = 2 \times 10^4$. The conversion efficiency of jet power into nonthermal electrons is $\bar{\epsilon} = \epsilon_{\rm e}\epsilon_{\rm th} = 0.3$, and $\epsilon_{\rm rad}$ is estimated according to the cooling regime (see Table 1). In all panels, vertical lines indicate transition LFs: Γ_τ (white dashed, Equation (8)), $\Gamma_{\rm c1}$ (green dotted–dashed, Equation (9)), and $\Gamma_{\rm cm}$ (purple dashed, Equation (10)), separating (shaded) regions of subphotospheric (gray), VFC (red), FC (green), and SC (purple). In all panels, the vertical dashed orange line indicates the critical LF $\Gamma_{\rm switch}$ where the cooling break equals the self-absorption frequency. In both bottom panels, the different shading of orange indicates the PLSs where the optical emission ($h\nu_{\rm opt} = 2$ eV) lies (notation following J. Granot & R. Sari 2002). The lighter gray shaded region (in the Thomson-thick regime) and white space (in the Thomson-thin regime) below the cyclotron photon energy denote that there is no emission below it. Left: the top left panel shows (in comoving frame) the minimal electron LF $\gamma_{\rm m}$ (horizontal dotted–dashed cyan), cooling LF $\gamma_{\rm c}$ (solid red), LF of particles contributing to self-absorption $\gamma_{\rm sa}$ (dashed blue), and modified cooling LF $\bar{\gamma}_{\rm c}$ (dotted black; see Equation (7) and Table 2) as a function of the bulk LF. Middle left panel: the prompt optical (2 eV) luminosity $(\nu L_\nu)_{\rm 2eV}$ (solid orange). The horizontal dotted–dashed orange line shows $(\nu L_\nu)_{\rm max} = L_{\rm iso}/\mathcal{W}$, with $\mathcal{W} = 7$ (see Appendix E; mean of $W(p = 2.5) = 6$ for FC/VFC and G $(p = 2.5) = 8$ for SC/VSC). Bottom left panel: the critical photon energies $h\nu_{\rm m}$ (dotted–dashed cyan), $h\nu_{\rm c}$ (solid red), $h\nu_{\rm sa}$ (dashed blue), and $h\nu_{\rm B}$ (dotted black); the horizontal orange line marks the optical band ($h\nu_{\rm opt} = 2$ eV). Right: the top right panel shows the combined dissipation and nonthermal electron acceleration efficiency, $\bar{\epsilon} = \epsilon_{\rm e}\epsilon_{\rm th}$ (solid red), and the radiative efficiency $\epsilon_{\rm rad}$ (dotted–dashed purple). Middle right panel: the isotropic jet luminosity $L_{\rm j,iso}$ for our assumed $L_{\rm iso}$ (dotted–dashed blue). Bottom right panel: the spectral index $\alpha_{\rm 2eV}$ (in dotted blue) in the optical band (at $h\nu_{\rm opt} = 2$ eV).

Figure 2 illustrates the parameter space favorable for bright prompt optical emission accompanying the prompt phase of GRBs, assuming a fixed observed isotropic luminosity $L_{\rm iso}$ with a spectral peak in the sub-MeV-to-MeV range, characteristic time variability $t_{\rm vz}$, and fixed jet and microphysical parameters (σ, ϵ, p, $\gamma_{\rm m}$). Both the VFC and FC regimes hold for a broad region of parameter space within the Thomson-thin domain where a luminous prompt optical counterpart can be realized. The VFC self-absorption photon energy $E_{\rm sa,8}(\Gamma_\tau < \Gamma < \Gamma_{\rm c1})$ (for other regimes, see Appendix E) is given as (for $p = 2.5$)

$$E_{\rm sa,8} \approx 2.5\, \Gamma_2^{-\frac{3}{2}}\, \gamma_{\rm m}^{-\frac{1}{3}}\, L_{52}^{\frac{1}{3}}\, f_{0.3}^{-\frac{2}{3}}\, t_{-1}^{-\frac{2}{3}}\ {\rm eV}\,, \tag{11}$$

which lies in the optical part of the electromagnetic spectrum. In general, the frequency of self-absorption is dependent on the power-law index p (see Appendix E). However, for $p = 2.5$, as has been used here for illustration, the dependence is very weak.

Figure 2 shows how prompt optical emission varies with the outflow's bulk LF, Γ. When $\nu_{\rm sa} > \nu_{\rm c}$, optical flux is suppressed by synchrotron self-absorption VFC regimes. For low Γ in the VFC regime, $\nu_{\rm opt} < \nu_{\rm sa}$, placing the optical band in the self-absorbed region of the synchrotron spectrum and yielding a characteristic spectral slope of $11/8$ (J. Granot et al. 2000). For higher values of Γ in both the VFC and FC regimes, as $\nu_{\rm sa}$ decreases with increasing Γ, the optical band transitions from self-absorbed ($\nu_{\rm opt} < \nu_{\rm sa}$) to optically thin ($\nu_{\rm opt} > \nu_{\rm sa}$). As $\nu_{\rm sa}$ approaches $\nu_{\rm c}$, the gap between spectral breaks narrows. When $\nu_{\rm sa} \sim \nu_{\rm c} \sim \nu_{\rm opt}$, the synchrotron spectrum approximates an unbroken power law across ~5–6 orders of magnitude in photon energy—from the sub-MeV peak to the optical band—producing a peak in optical luminosity within the FC regime. Once $\nu_{\rm sa} \lesssim \nu_{\rm opt} < \nu_{\rm c}$, the optical spectral slope approaches the value $1/3$ (i.e., $\Gamma > \Gamma_{\rm switch}$) and self-absorption no longer significantly affects the optical band, but the flux diminishes as the cooling break moves to higher frequencies. In the SC regime, where $\nu_{\rm c} \gg \nu_{\rm m} \gg \nu_{\rm opt}$, the optical emission weakens further due to the low radiative efficiency $\epsilon_{\rm rad}$ and the increasing frequency gap between the peak of the bolometric luminosity at $\nu_{\rm c}$ and the optical band at $\nu_{\rm opt}$.

To summarize the principal findings of this section, bright prompt optical emission from GRBs is most plausibly produced in the VFC and FC regimes of optically thin synchrotron radiation. The VFC regime favors emission in both the self-absorbed domain with a spectral slope of $11/8$ at lower LF and the optically thin domain with a spectral slope of $-1/2$ at higher LF. The FC regime permits optically thin

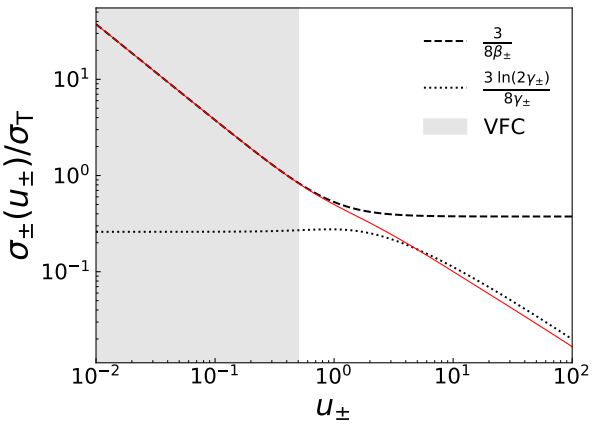

Figure 3. Annihilation cross section of electron–positron pairs (see Equation (12)), shown in red, as a function of the proper speed of the recombining pairs. Dashed and dotted segments show the asymptotic behavior at the low- and high-proper-speed regimes, respectively. The VFC regime is indicated by the shaded gray region.

contributions with a spectral slope of both $-1/2$ at lower LF and $1/3$ at higher LF. In contrast, the SC regime is the least favorable for producing a bright optical counterpart during the prompt phase, as it is also associated with diminished gamma-ray emission. In the next section, we explore the observable implication of VFC in the Thomson-thick (subphotospheric) domain.

4. Multi-MeV Spectral Line in GRB 221009A

Here we examine the role of VFC in the *Thomson-thick*, subphotospheric regime (gray shaded region in Figure 2) in the context of the recent observation of a multi-MeV bright spectral emission line (E. Burns et al. 2024; M. E. Ravasio et al. 2024; M. Axelsson et al. 2025) associated with the prompt phase of GRB 221009A (aka the B.O.A.T.). This feature is commonly interpreted as an electron–positron annihilation line. The formation of such a spectral line occurs through a two-step process. First, high-energy continuum photons undergo $\gamma\gamma$ attenuation, producing electron–positron pairs. Next, these pairs must recombine and annihilate to generate the spectral line. The recombination efficiency is influenced by the cross section, which depends on the velocity of the recombining particles, $\beta_\pm c$ (W. Heitler 1954):

$$\frac{\sigma_\pm(u_\pm)}{\sigma_T} = \frac{3/8}{\beta_\pm u_\pm(\gamma_\pm+1)} \times\left[\left(\gamma_\pm+4+\frac{1}{\gamma_\pm}\right)\ln(\gamma_\pm+u_\pm)-\beta_\pm(\gamma_\pm+3)\right] \approx\begin{cases}\dfrac{3}{8\beta_\pm} & \text{for } u_\pm \ll 1,\\ [8pt]\dfrac{3\ln(2\gamma_\pm)}{8\gamma_\pm} & \text{for } u_\pm \gg 1.\end{cases} \tag{12}$$

Figure 3 shows that the annihilation cross section is maximized when the recombining electron–positron pairs are nonrelativistic in the bulk frame. The same condition is required for the line to be locally narrow in the comoving frame (centered at $h\nu'_{\rm line} = m_e c^2$). From Equation (9), the critical LF below which the VFC can be invoked in GRB 221009A is $\Gamma \leqslant \Gamma_{c1} \sim 245$ (for $L_{54} = L_{\rm iso}/10^{54}$ erg s^{-1} and $t_{0.9} = t_{\rm vz}/8$ s from D. Frederiks et al. 2023). This shows that models (A. Pe'er & B. Zhang 2024; Z. Zhang et al. 2024) that invoke bulk jet LF $\Gamma \gtrsim 400$ will not be able to produce a bright and narrow electron–positron annihilation line. A detailed exploration for the formation and subsequent escape of this bright line is being pursued in a separate follow-up work.

To summarize, the VFC is a necessary requirement for the formation of the narrow and bright annihilation line in GRB 221009A.

5. Cooling Regimes in Magnetic Reconnection Events

In this section, we qualitatively comment on how VFC (or FC or SC) can play an important role in radiatively enhanced models of magnetic reconnection. Reconnection models naturally involve a magnetically dominated emission region. This typically leads to synchrotron being the dominant radiation process and tends to result in FC or VFC electrons (P. Beniamini & T. Piran 2014; P. Beniamini & J. Granot 2016). Most reconnection-based models assume a constant reconnection rate. Although several studies include the effects of radiative cooling (C. H. Jaroschek & M. Hoshino 2009; D. A. Uzdensky & J. C. McKinney 2011; B. Cerutti et al. 2014; K. Nalewajko et al. 2018; H. Hakobyan et al. 2023; K. M. Schoeffler et al. 2023), they typically find that the reconnection rate remains enhanced but effectively constant, with the reconnection layer maintaining the pressure balance between the magnetic pressure of the incoming cold plasma and the thermal pressure of the hot outflowing accelerated particles in the thin reconnection layer. However, in the VFC regime, radiative losses can become so severe that they disrupt this pressure balance: particles cool rapidly before they can provide sufficient thermal support, resulting in a significant pressure drop within the layer. This breakdown of pressure equilibrium could, in principle, further accelerate reconnection beyond the rates reported in previous studies.

The effect of radiative cooling also depends on the composition of the plasma and hardness of the particle distribution. In reconnection events, the initial magnetic field energy density is transferred into the charged particle species —either electron–positron or electron–ion—postreconnection. For electron–positron plasmas, FC is sufficient, as even relativistic cooling LFs result in significant energy and thermal pressure loss, which strongly affects the reconnection dynamics. In electron–ion plasmas, however, since ions do not radiate efficiently and typically hold at least half of the postreconnection internal energy, the drop in internal energy is at most by a factor of $\sim$2 (for VFC, FC, or SC with $p < 2$; in the other regimes, even the electrons keep most of their initial internal energy), leading to a more modest effect on the reconnection dynamics. Notably, SC can lead to substantial energy loss for harder particle spectra (SC with $p < 2$; see Table 1), where high-energy electrons dominate the total nonthermal energy, with a cooling timescale $t'_{\rm cM}$.

6. Conclusion

The main objective of this study is to explore the generic synchrotron cooling parameter space of nonthermal particles with a special emphasis on positioning the VFC regime within the broader context of particle cooling mechanisms. We find this regime particularly relevant to highly luminous relativistic outflows such as the prompt phase of GRBs, regardless of the

specifics of the dissipation process. While this work focused on synchrotron losses only, additional radiative channels, such as synchrotron self-Compton, would work to make cooling more efficient and could increase the available parameter space for the FC and VFC regimes.

As example, inverse Compton (IC) scattering can be incorporated through a generalized Compton parameter (e.g., following J. Granot & A. Königl 2001), $Y = Y_{\rm SSC} + Y_{\rm ext}$, where $Y_{\rm SSC} = u_{\rm syn}/u_{\rm B}$ and $Y_{\rm ext} = u_{\rm ext}/u_{\rm B}$. Here, $u_{\rm syn}$, $u_{\rm ext}$, and $u_{\rm B}$ denote the comoving energy densities of synchrotron photons, external photons, and the magnetic field, respectively. This formulation is particularly relevant in models of tidal disruption events (e.g., P. Kumar et al. 2013), where IC cooling of electrons in the external shock by internally produced photons (external to the shocked region) may play a significant role. The presence of such additional cooling channels modifies the electron cooling timescale $t'_{\rm c1}$ (see, e.g., Equation (12) of P. Beniamini & T. Piran 2013) and thus the generalized cooling LF $\tilde{\gamma}_{\rm c}$. As discussed in J. Granot & R. Sari (2002), the effect of IC cooling on the synchrotron spectrum can be captured by multiplying the flux density in the relevant power-law segments (PLSs) of the synchrotron spectral energy distribution (SED) by appropriate powers of $(1 + Y)$, thereby accounting for the enhanced cooling efficiency.

Our analysis suggests that VFC in the optically thick regime is essential to explaining the origin of the bright electron–positron annihilation line observed in GRB 221009A. In certain standard prompt-GRB parameter spaces, we show that self-absorption in the FC–VFC regime can occur near the cooling break, allowing for bright UV/optical emission with an unbroken power-law spectrum extending from the gamma-ray peak energy down to UV/optical frequencies.

Furthermore, the VFC regime has potential applications in relativistic magnetic reconnection models, where it may accelerate the reconnection rate by altering the pressure balance within the reconnection layers.

What sets the VFC regime apart from other cooling regimes is its unique characteristic: injected electrons cool to nonrelativistic speeds on timescales much shorter than the dynamical timescale. We encourage further exploration of this distinctive feature of VFC cooling. In an accompanying study, we investigate this regime in detail, with the objective of reproducing the temporal signature of the electron–positron annihilation line observed in B. O.A.T. GRB 221009A. Although our analysis here is based on synchrotron cooling, the framework can be easily adapted to other radiative cooling processes.

Acknowledgments

P.B. is supported by a grant (No. 2020747) from the United States–Israel Binational Science Foundation (BSF), Jerusalem, Israel; a grant (No. 1649/23) from the Israel Science Foundation; and a grant (No. 80NSSC 24K0770) from the NASA Astrophysics Theory Program.

Appendix A
Cooling Timescales

The purpose of this section is to motivate the definition of $t'_{\rm c1} \equiv \frac{6\pi m_{\rm e} c}{\sigma_{\rm T} B'^2}$ as the synchrotron cooling timescale associated with a mildly relativistic electron.

We consider the synchrotron cooling of a relativistic electron slowing down to a nonrelativistic velocity in a homogeneous and uniform magnetic field, B'. For simplicity, we will use the mean cooling rate per particle for an isotropic distribution of velocities. The energy loss of the particle is governed by the equation (L. D. Landau & E. M. Lifshitz 1975)

$$\frac{d}{dt'}(\gamma m_{\rm e} c^2) = -\frac{\sigma_{\rm T} c}{6\pi} B'^2 \gamma^2 \beta^2 = -\frac{\sigma_{\rm T} c}{6\pi} B'^2 (\gamma^2 - 1). \quad \text{(A1)}$$

This equation can be integrated to find the LF, $\gamma_{\rm f}$, as a function of comoving time t', as follows:

$$\int_{\gamma_{\rm i}}^{\gamma} \frac{d\gamma}{\gamma^2 - 1} = -\frac{t'}{t'_{\rm c1}} \Rightarrow \gamma - 1 = \frac{2\left(\frac{\gamma_{\rm i} - 1}{\gamma_{\rm i} + 1}\right)}{e^{\frac{2t'}{t'_{\rm c1}}} - \left(\frac{\gamma_{\rm i} - 1}{\gamma_{\rm i} + 1}\right)}$$

$$\approx \begin{cases} \dfrac{\gamma_{\rm i} - 1}{1 + \frac{t'}{t'_{\rm c1}/\gamma_{\rm i}}} & \text{for } \gamma_{\rm i} \gg 1 \ \ \& \ \ t' \ll t'_{\rm c1} \\ 2\, e^{-\frac{2t'}{t'_{\rm c1}}} & \text{for } \gamma_{\rm i} \gg 1 \ \ \& \ \ t' \gg t'_{\rm c1} \end{cases}, \quad \text{(A2)}$$

where $t'_{\rm c1} = \frac{6\pi m_{\rm e} c}{\sigma_{\rm T} B'^2}$.

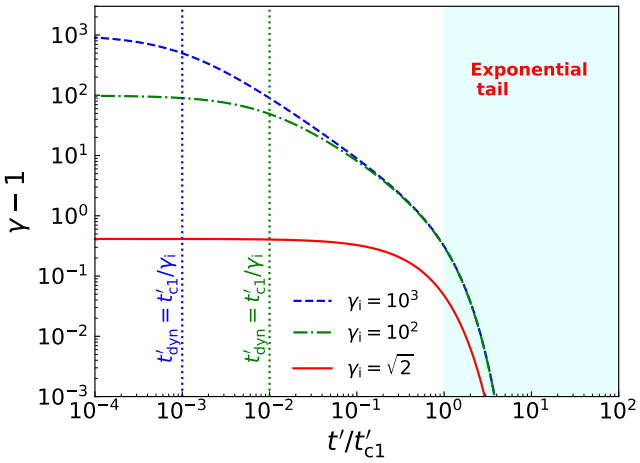

Figure 4. Synchrotron cooling of a charged particle with an initial LF $\gamma_{\rm i}$ in a homogeneous comoving magnetic field B'. The figure depicts the evolution of the particle's kinetic energy, normalized by its rest-mass energy $m_{\rm e}c^2$, i.e., $\gamma - 1$, as a function of comoving time t', normalized by the characteristic comoving timescale $t'_{\rm c1}$. The dotted blue, dotted–dashed green, and solid red lines correspond to initial LFs $\gamma_{\rm i}$ of 10^3, 10^2, and $\sqrt{2}$, respectively. The vertical dotted blue and green lines indicate the cooling timescales $t'_{\rm c}$ at which the electron cools to half of its initial LF. The shaded cyan region marks the phase where electron cooling transitions from the power-law decay regime into the exponential regime, characterized by the timescale $t'_{\rm c1}/2$.

Figure 4 shows the synchrotron cooling of an electron as a function of the comoving time t'. An initially relativistic electron with an initial LF $\gamma_{\rm i} \gg 1$ undergoes three distinct stages of cooling. In the first stage, for $t' \ll t'_{\rm c1}/\gamma_{\rm i}$, the electron hardly cools, and its LF remains approximately constant, $\gamma_{\rm e} \approx \gamma_{\rm i}$. At $t' = t'_{\rm c1}/\gamma_{\rm i}$, the electron cools to $\gamma_{\rm e} = \gamma_{\rm i}/2$, meaning that roughly half of the initial energy is radiated away. In the second stage, for $\gamma_{\rm i}^{-1} < t'/t'_{\rm c1} < 1$, the electron cools significantly with $\gamma_{\rm e} \propto 1/t'$ while remaining relativistic. Finally, for $t' > t'_{\rm c1}$, the electron cools to a nonrelativistic velocity, with its velocity decaying exponentially over a characteristic timescale of $t'_{\rm c1}/2$. In the case of a single electron with a fixed initial LF $\gamma_{\rm i}$, these cooling stages are well defined. For $t'_{\rm dyn} \ll t'_{\rm c1}$, cooling is inversely proportional to the initial LF,

and at $t' = t'_{\rm dyn}$, the final LF is $\gamma_{\rm f} = \gamma_{\rm i}/2$. In contrast, for $t'_{\rm dyn} \gg t'_{\rm c1}$, the electron cools exponentially to a nonrelativistic velocity, with cooling becoming independent of the initial LF. In this scenario, any large initial LF must first cool to a mildly relativistic regime before transitioning into the nonrelativistic domain (where it loses the memory of the initial LF $\gamma_{\rm i}$); the characteristic cooling timescale $t'_{\rm c1}$ can then be defined as the cooling timescale for a mildly relativistic particle.

Appendix B
Summary of Photon and Particle Spectrum in the Cooling Regimes

In this section, we derive the general expression for the radiative efficiency $\epsilon_{\rm rad}$ assuming synchrotron cooling over one dynamical timescale, starting from an initial distribution given by Equation (1). The efficiency is defined as

$$\epsilon_{\rm rad} = 1 - \frac{E_{\rm f}}{E_{\rm i}}, \tag{B1}$$

where the initial and final energies (for relativistic electrons) are given by

$$\frac{E_{\rm i}}{m_{\rm e}c^2} = \int d\gamma_{\rm i}\, \frac{dN}{d\gamma_{\rm i}} \gamma_{\rm i}\ , \qquad \frac{E_{\rm f}}{m_{\rm e}c^2} = \int d\gamma_{\rm i}\, \frac{dN}{d\gamma_{\rm i}}\, \gamma_{\rm f}\ , \tag{B2}$$

with the cooled LF

$$\gamma_{\rm f} = \frac{\gamma_{\rm i}\bar{\gamma}_{\rm c}}{\gamma_{\rm i} + \bar{\gamma}_{\rm c}}\ , \qquad \bar{\gamma}_{\rm c} = \frac{t'_{\rm c1}}{t'_{\rm dyn}}\ . \tag{B3}$$

For a power-law distribution between $\gamma_{\rm m}$ and $\gamma_{\rm M}$ with index p, the radiative efficiency becomes

$$\epsilon_{\rm rad} = 1 - \frac{p-2}{\gamma_{\rm m}^{2-p} - \gamma_{\rm M}^{2-p}} I, \tag{B4}$$

where

$$I = \int_{\gamma_{\rm m}}^{\gamma_{\rm M}} d\gamma_{\rm i}\, \frac{\gamma_{\rm i}^{1-p}\bar{\gamma}_{\rm c}}{\gamma_{\rm i} + \bar{\gamma}_{\rm c}}. \tag{B5}$$

Evaluating the integral, we obtain

$$I = (p-2)\bar{\gamma}_{\rm c}^2 \frac{-\gamma_{\rm m}^{-p}\left(-\frac{\gamma_{\rm m}}{\bar{\gamma}_{\rm c}}\right)^p B\left(-\frac{\gamma_{\rm m}}{\bar{\gamma}_{\rm c}}, 2-p, 0\right) + \gamma_{\rm M}^{-p}\left(-\frac{\gamma_{\rm M}}{\bar{\gamma}_{\rm c}}\right)^p B\left(-\frac{\gamma_{\rm M}}{\bar{\gamma}_{\rm c}}, 2-p, 0\right)}{\gamma_{\rm m}^{2-p} - \gamma_{\rm M}^{2-p}}, \tag{B6}$$

where the generalized cooling LF $\bar{\gamma}_{\rm c}$ for different cooling regimes is summarized in Table 2. The incomplete beta function is defined as

$$B(x, a, 0) = \int_0^x du\, \frac{u^{a-1}}{1-u}. \tag{B7}$$

Table 1 presents a concise summary of the different cooling regimes, while Figure 5 provides a comparative illustration of the analytical expression for the radiative efficiency and its corresponding power-law approximation (as summarized in Table 1).

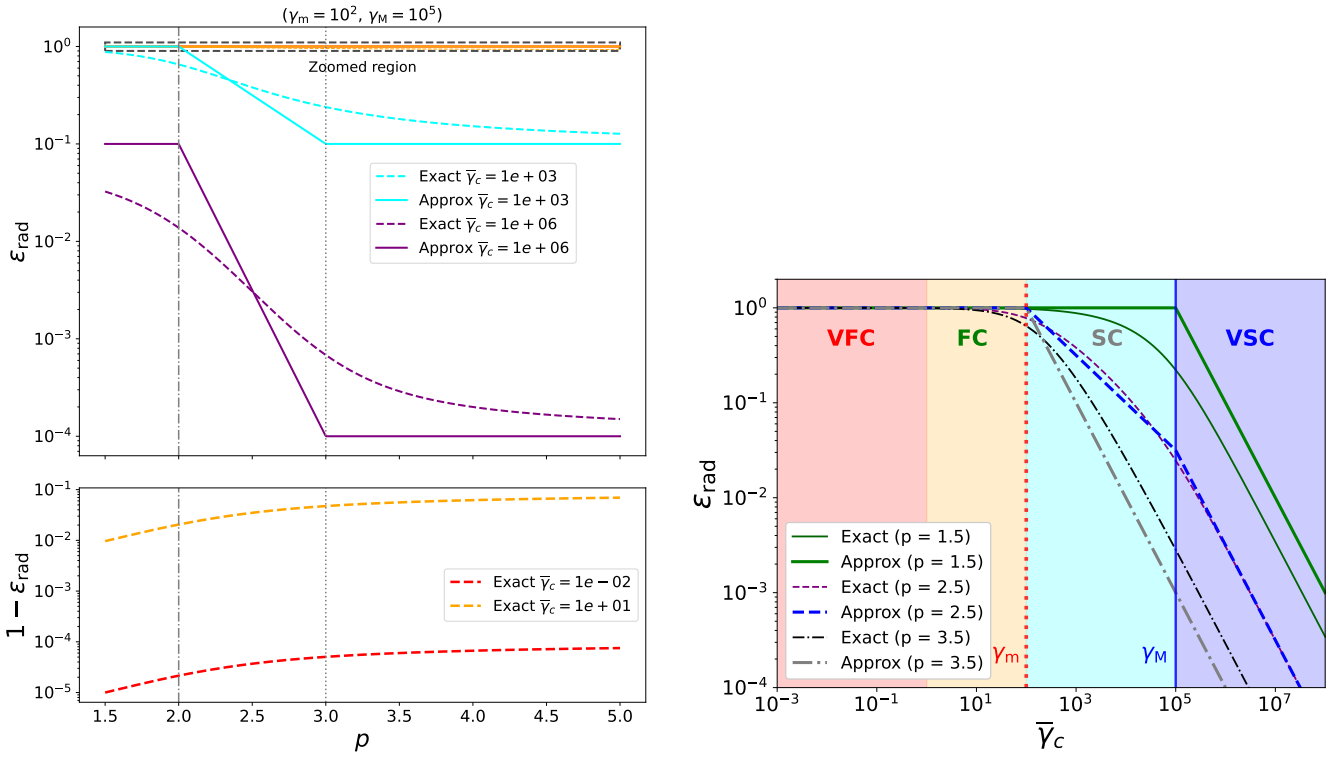

Figure 5. Comparison of the radiative efficiency, ϵ_{rad}, between the exact analytical expression and the power-law approximation (as summarized in Table 1). In both panels, we adopt $(\gamma_m, \gamma_M) = (10^2,\ 10^5)$. The color scheme denotes different cooling regimes: red for VFC, orange for FC, cyan for SC, and purple for VSC. Left panel: radiative efficiency is shown as a function of the power-law index p on a semilogarithmic scale. Dashed lines represent the exact analytical solution, and solid lines correspond to the power-law approximation. Each curve represents a different value of the generalized cooling Lorentz factor $\bar{\gamma}_c$, highlighting transitions across cooling regimes. The lower subplot provides a linear-scale zoom-in of the exact analytical solution FC and VFC regimes for clarity (for these regimes, the power-law approximation is $\epsilon_{rad} = 1$). Right panel: radiative efficiency is plotted against $\bar{\gamma}_c$ on a log–log scale. Thinner lines indicate the analytical solution, and thicker lines represent the power-law approximation for different values of p. Colors distinguish p values: dark and light green for $p = 1.5$, purple and blue for $p = 2.5$, and black and gray for $p = 3.5$.

Appendix C
Implausibility of VFC in Newtonian Regime

The objective of this section is to explore the possibility of VFC arising in Newtonian outflows. Let E be the internal energy contained within a spherical Newtonian outflow expanding at a constant velocity v. The outer radius of the outflow at any given time t is $R = vt$. We assume that a generic dissipation process converts a fraction ϵ_{diss} of the total energy into internal energy $E_{int} = \epsilon_{diss}E$. Assuming that a fraction ϵ_e of E_{int} goes into the energy of nonthermal electrons, we have $E_e = \epsilon_e E_{int}$. Assuming that a fraction ϵ_B of E_{int} goes into the magnetic field, we have $E_B = \epsilon_B E_{int}$. The cooling LF $\bar{\gamma}_c$ can then be expressed as

$$\bar{\gamma}_c = \frac{\pi m_e c}{\sigma_T}\ \epsilon_{diss}^{-1}\ \epsilon_e^{-1}\ \epsilon_B^{-1}\ v^3\ t^2\ E^{-1}$$
$$\approx 3.6\ \epsilon_{diss,-0.3}^{-1}\ \epsilon_{e,-1}^{-1}\ \epsilon_{B,-1}^{-1}\ v_8^3\ t_1^2\ E_{51}^{-1}, \quad \text{(C1)}$$

where $\epsilon_{diss,-0.5} = \epsilon_{disp}/0.5$, $\epsilon_{e,-1} = \epsilon_e/0.1$, $\epsilon_{B,-1} = \epsilon_B/0.1$, $v_8 = v/10^8$ cm s^{-1}, $t_1 = t/10$ yr, and $E_{51} = 10^{51}$ erg.

Equation (C1) demonstrates that even for a highly energetic Newtonian outflow at a very young age, with dissipation efficiencies pushed to very high values, the cooling LF does not drop below unity. This indicates that VFC is unlikely to occur in Newtonian outflows. A further complication is that at very young ages, the Thomson optical depth is very high. This can be represented as (assuming χ_{ion} is the ionization fraction in the outflow)

$$\tau_T = \frac{3\sigma_T}{2\pi m_p}\ \chi_{ion}\ v^{-4}\ t^{-2}\ E$$
$$\approx 5.73\ \chi_{ion,-0.5}\ v_8^{-4}\ t_1^{-2}\ E_{51}\ , \quad \text{(C2)}$$

where $\chi_{ion,-0.5} = \chi_{ion}/0.3$.

Multiplying Equation (C2) and Equation (C1), we obtain

$$\bar{\gamma}_c \tau_T = \frac{3}{2}\frac{m_e}{m_p}\frac{c}{v}\ \epsilon_{diss}^{-1}\ \epsilon_e^{-1}\ \epsilon_B^{-1}\ \chi_{ion}$$
$$\approx 14.8\ \chi_{ion,-0.4}\ \epsilon_{diss,-0.3^{-1}}\ \epsilon_{e,-1^{-1}}\ \epsilon_{B,-1^{-1}}\ v_8^{-1}, \quad \text{(C3)}$$

which shows that the cooling LF $\bar{\gamma}_c$ and the Thomson optical depth τ_T are inversely related in terms of their dependence on the core underlying parameters, meaning that any attempt to reduce $\bar{\gamma}_c$ comes at the expense of an increase in the optical depth of the outflow. This implies that optically thin VFC in Newtonian outflows is highly improbable.

Appendix D
Distinguishing One-zone and Shock-heated Models of Nonthermal Electrons

In this section, we distinguish between the one-zone model (G. Ghisellini et al. 1988; H. Gao et al. 2013) and the shock-

heated model (J. Granot et al. 2000; J. Granot & R. Sari 2002) of particle acceleration and cooling in relativistic jets. In the former model, electrons are assumed to be continuously and uniformly injected in the entire emission region. In such models, pileup arises uniformly in the emission region, below an electron LF $\gamma_{\rm sa}$, where synchrotron cooling losses are balanced by self-absorption gains. These piled-up electrons reach a quasi-Maxwellian energy distribution below $\gamma_{\rm sa}$ at mildly relativistic/subrelativistic velocities,[5] which leads to a low-frequency thermal bump below the self-absorption frequency $\nu_{\rm sa}$ superimposed on the nonthermal spectrum. A distinctive observational prediction of these models is a ν^2 SED below the self-absorption frequency (for $\nu < \nu_{\rm sa} < \nu_m$ in the strong self-absorption regime where $\nu_c < \nu_{\rm sa}$). However, it must be noted that the thermal bump in the SED can only be modest, as it depends logarithmically on the particle number excess or pileup (see Figures 1 and 2 of G. Ghisellini et al. 1988).

In the latter model of shock heating, electrons are locally accelerated at a very thin shock front and subsequently predominantly advected downstream away from the shock front, such that the time over which they cool is proportional to their distance behind the shock front, such that $l'_c(\gamma_e) = l'_0 \frac{\gamma_m}{\gamma_e}$, where $l'_0 \equiv l'_c(\gamma_m)$, while at distances $l' > l'_0$, all electrons have cooled significantly to a locally nearly monoenergetic energy distribution, $\frac{dn_e}{d\gamma_e}(l' > l'_0) \approx n_e \delta(\gamma_e - \gamma_m l'_0/l')$. The latter is relevant only for FC or VFC where $l'_0 < l'_{\rm dyn} \sim R/c\Gamma$ (while for SC or VSC, $l'_0 > l'_{\rm dyn}$, rendering l'_0 irrelevant). Consequently, the observed emission for FC or VFC is highly sensitive to the spatial distribution of electrons relative to the shock front. Below $\nu_{\rm sa}$, the emission at each observed frequency ν arises from a region of optical depth (to self-absorption) close to unity, which is located at a frequency-dependent distance l'_1 behind the shock, defined by the condition $\tau_\nu(l'_1) = 1$ (where the observer is assumed to be located in front of the shock, such that $\tau_\nu(l' = 0) = 0$). For FC or VFC, one can define a transition frequency $\nu_{\rm ac}$ satisfying $l'_1(\nu_{\rm ac}) = l'_0$, below which $l'_1 < l'_0$ and the emission (at $\nu < \nu_m$) is dominated by uncooled electrons with $\gamma_e \sim \gamma_m$, leading to $F_\nu \propto \nu^2$. The distance l'_1 increases with frequency, where for $\nu > \nu_{\rm ac}$, it scales as $l'_1 \propto \nu^{5/8}$ and satisfies $l'_1 > l'_0$ such that the emission arises from significantly cooled electrons with $\gamma_e(l'_1) \propto 1/l'_1 \propto \nu^{-5/8}$ leading to $F_\nu \propto \nu^2 \gamma_e(l'_1) \propto \nu^{11/8}$ for $\nu_{\rm ac} < \nu < \nu_{\rm sa}$. This $\nu^{11/8}$ spectral slope is a distinctive feature of such a stratified cooling structure, which arises in both the FC and VFC regimes.

In the shock-heated model, pileup can potentially occur only at $l' > l'_1(\gamma_{\rm sa})$ (where $\gamma_{\rm sa} \gg 1$), while the emission always arises from $l'_1 \leqslant l'_1(\gamma_{\rm sa})$; therefore, the emission would hardly be affected by such pileup, even if it does occur (since the emission arises from closer to the shock front).

Appendix E
Self-absorption Effects in Prompt GRBs

Consider a relativistic source of radius R and LF Γ that emits synchrotron radiation at a distance d subtending a solid angle $\Delta\Omega = A_{\rm eff}/d^2$ (where $A_{\rm eff} = \pi R^2/\Gamma^2$ corresponds to a transverse radial width R/Γ) toward the observer. For synchrotron radiation, the isotropic bolometric luminosity $L_{\rm iso}$ can be expressed as (for $2 < p < 3$)

$$L_{\rm iso} = \mathcal{W}(p)(\nu L_\nu)_{\rm max} = \begin{cases} \frac{2(p-1)}{(p-2)} \nu_{\rm m} L_{\nu_{\rm m}} & \text{FC and VFC} \\ \frac{2}{(p-2)(3-p)} \nu_{\rm c} L_{\nu_{\rm c}} & \text{SC} \end{cases}, \tag{E1}$$

where $\mathcal{W}$ is a numerical factor, $(\nu L_\nu)_{\rm max}$ is the peak of the bolometric luminosity, and $\nu_{\rm m}$ and $\nu_{\rm c}$ are the minimal and cooling synchrotron frequencies, respectively.

At the self-absorption frequency $\nu_{\rm sa}$, the following relationship holds:

$$\frac{2kT_{\rm eff}}{c^2} \nu_{\rm sa}^2 \Delta\Omega = \frac{L_{\nu_{\rm sa}}}{4\pi d^2}, \tag{E2}$$

such that $kT_{\rm eff} = \Gamma \gamma_{\rm sa} m_{\rm e} c^2$, where $\gamma_{\rm sa}$ is the LF of the self-absorbing particles.

Table 3 compares the notation in our work with that of J.Granot & R. Sari (2002). The self-absorption frequency in the different cooling regimes can be summarized as

$$\nu_{\rm sa} = \begin{cases} \nu_{\rm sa,1} = \left[\frac{1}{m_{\rm e}} \frac{1}{8\pi^2 R^2} \frac{1}{\gamma_{\rm m}} \frac{\Gamma L_{\rm iso}}{\mathcal{W}}\right]^{\frac{3}{5}} \nu_{\rm c}^{\frac{3p-9}{10}} \nu_{\rm m}^{\frac{1-3p}{10}} & \text{for } \nu_{\rm sa,1} < \nu_{\rm m} \text{ (spectrum 1: SC)}, \\ \nu_{\rm sa,8} \equiv \left[\frac{1}{m_{\rm e}} \frac{1}{8\pi^2 R^2} \frac{1}{\gamma_{\rm m}} \frac{\Gamma L_{\rm iso}}{\mathcal{W}}\right]^{\frac{1}{3}} \left(\frac{\nu_{\rm m}}{\nu_{\rm c}}\right)^{\frac{2-p}{6}} & \text{for } \nu_{\rm sa,8} > \nu_{\rm c} \text{ (spectrum 4: FC and VFC)}, \\ \nu_{\rm sa,10} = \left[\frac{1}{m_{\rm e}} \frac{1}{8\pi^2 R^2} \frac{1}{\gamma_{\rm m}} \frac{\Gamma L_{\rm iso}}{\mathcal{W}}\right]^{\frac{3}{5}} \nu_{\rm m}^{\frac{6-3p}{10}} \nu_{\rm c}^{\frac{3p-14}{10}} & \text{for } \nu_{\rm sa,10} < \nu_{\rm c} \text{ (spectrum 5: FC and VFC)}, \end{cases} \tag{E3}$$

where the self-absorption frequencies ($\nu_{\rm sa,1}$, $\nu_{\rm sa,8}$, $\nu_{\rm sa,10}$) follows the closure relationships ($\nu_{\rm sa,8} \approx \nu_1^{\frac{5}{9}} \nu_2^{\frac{5}{18}} \nu_3^{\frac{1}{6}}$, $\nu_{\rm sa,10} \approx \nu_1 \left(\frac{\nu_2}{\nu_3}\right)^{\frac{1}{2}}$) (where ν_1, ν_2, and ν_3 correspond to $\nu_{\rm sa,1}$,

[5] If the electrons are relativistic with $\gamma_{\rm e} \gg 1$, then IC (and specifically synchrotron self-Compton) would increase the frequency by a factor of $\sim\gamma_{\rm e}^2 \gg 1$ where it is optically thin and can freely escape, leading to efficient cooling and thus avoiding significant pileup. H. Gao et al. (2013) do not appear to take this point into account, and G. Ghisellini et al. (1988) do not consider IC cooling.

Table 3
Corresponding Symbols in Our Work and J. Granot & R. Sari (2002)

Our Work	J. Granot & R. Sari (2002)	Meaning
$\nu_{\rm sa,1}$	ν_1	Self-absorption frequency in spectrum 1 (SC)
$\nu_{\rm sa,8}$	ν_8	Self-absorption frequency in spectrum 4 (FC and VFC)
$\nu_{\rm sa,10}$	ν_{10}	Self-absorption frequency in spectrum 5 (FC and VFC)

$\nu_{\rm m}$, and $\nu_{\rm c}$ in spectrum 1) as discussed J. Granot & R. Sari (2002). The minimal and the cooling frequency are given as

$$\nu_{\rm m} \approx \Gamma\gamma_{\rm m}^2\nu'_{\rm B} = \frac{\gamma_{\rm m}^2}{2\pi m_{\rm e}c}\frac{1}{R}\sqrt{\frac{\sigma}{1+\sigma}\frac{L_{\rm iso}}{c\epsilon}}, \tag{E4}$$

$$\nu_{\rm c} \approx \Gamma\gamma_{\rm c}^2\nu'_{\rm B} = \frac{\gamma_{\rm c}^2}{2\pi m_{\rm e}c}\frac{1}{R}\sqrt{\frac{\sigma}{1+\sigma}\frac{L_{\rm iso}}{c\epsilon}}. \tag{E5}$$

ORCID iDs

Sk. Minhajur Rahaman https://orcid.org/0000-0003-1214-0521
Jonathan Granot https://orcid.org/0000-0001-8530-8941
Paz Beniamini https://orcid.org/0000-0001-7833-1043

References

Axelsson, M., Ajello, M., Arimoto, M., et al. 2025, ApJS, 277, 24
Beniamini, P., Barniol Duran, R., & Giannios, D. 2018, MNRAS, 476, 1785
Beniamini, P., & Granot, J. 2016, MNRAS, 459, 3635
Beniamini, P., & Piran, T. 2013, ApJ, 769, 69
Beniamini, P., & Piran, T. 2014, MNRAS, 445, 3892
Burns, E., Lesage, S., Goldstein, A., et al. 2024, arXiv:2410.00286
Cerutti, B., Werner, G. R., Uzdensky, D. A., & Begelman, M. C. 2014, ApJ, 782, 104
Daigne, F., Bošnjak, Ž., & Dubus, G. 2011, A&A, 526, A110
Frederiks, D., Svinkin, D., Lysenko, A. L., et al. 2023, ApJL, 949, L7
Gao, H., Lei, W.-H., Wu, X.-F., & Zhang, B. 2013, MNRAS, 435, 2520
Ghisellini, G., & Celotti, A. 1999, ApJL, 511, L93
Ghisellini, G., Guilbert, P. W., & Svensson, R. 1988, ApJL, 334, L5
Granot, J., & Königl, A. 2001, ApJ, 560, 145
Granot, J., Piran, T., & Sari, R. 2000a, ApJL, 534, L163
Granot, J., & Sari, R. 2002, ApJ, 568, 820
Guetta, D., & Granot, J. 2003, MNRAS, 340, 115
Hakobyan, H., Ripperda, B., & Philippov, A. A. 2023, ApJL, 943, L29
Heitler, W. 1954, Quantum Theory of Radiation (Oxford: Clarendon)
Jaroschek, C. H., & Hoshino, M. 2009, PhRvL, 103, 075002
Kumar, P., Barniol Duran, R., Bošnjak, Ž., & Piran, T. 2013, MNRAS, 434, 3078
Kumar, P., & McMahon, E. 2008, MNRAS, 384, 33
Landau, L. D., & Lifshitz, E. M. 1975, The Classical Theory of Fields (Oxford: Pergamon Press)
Nalewajko, K., Yuan, Y., & Chruślińska, M. 2018, JPlPh, 84, 755840301
Pe'er, A., & Zhang, B. 2024, ApJL, 973, L51
Rahaman, S. M., Granot, J., & Beniamini, P. 2024, MNRAS, 528, 160
Ravasio, M. E., Salafia, O. S., Oganesyan, G., et al. 2024, Sci, 385, 452
Sari, R., Piran, T., & Narayan, R. 1998, ApJL, 497, L17
Schoeffler, K. M., Grismayer, T., Uzdensky, D., & Silva, L. O. 2023, MNRAS, 523, 3812
Uzdensky, D. A., & McKinney, J. C. 2011, PhPl, 18, 042105
Zhang, Z., Lin, H., Li, Z., et al. 2024, ApJL, 973, L17